A preliminary version of this manuscript has been presented at the
6th International Conference on Tethers in Space (12–14 June 2019, Madrid, Spain).

Electric sail phasing maneuvers for constellation deployment

Lorenzo Niccolai*, Andrea Caruso, Alessandro A. Quarta, Giovanni Mengali

Dipartimento di Ingegneria Civile e Industriale, University of Pisa, I-56122, Italy

Abstract

The aim of this work is to investigate heliocentric phasing maneuvers performed by a spacecraft propelled by an Electric Solar Wind Sail, that is, an innovative propellantless propulsion system that consists of a spinning grid of charged tethers that uses solar wind momentum to produce thrust. It is assumed that the Electric Solar Wind Sail may be controlled by varying its attitude with respect to a classical orbital reference frame, and by switching the tether grid off to obtain Keplerian arcs along its phasing trajectory. The analysis is conducted within an optimal framework, the aim of which is to find both the optimal control law and the minimum-time phasing trajectory for a given angular drift along the (assigned) working orbit. A typical phasing scenario is analyzed, by considering either a drift ahead or a drift behind maneuver on a circular, heliocentric orbit of given radius. The paper also investigates the possibility of using an Electric Solar Wind Sail-based deployer to place a constellation of satellites on the same working orbit. In that case, the optimal flight time is obtained in a compact, semianalytical form as a function of both the propulsion system performance and the number of the sail-deployed satellites.

Keywords: Electric Solar Wind Sail, time-optimal phasing maneuver, constellation deployment

Nomenclature

$\boldsymbol{a}$	=	propulsive acceleration vector, [mm/s^2]
a_c	=	characteristic acceleration, [mm/s^2]
$\{a_r, a_\theta\}$	=	propulsive acceleration components, [mm/s^2]
$\{\hat{\boldsymbol{\imath}}_r, \hat{\boldsymbol{\imath}}_\theta\}$	=	polar reference frame unit vectors
$\mathcal{H}$	=	Hamiltonian function
J	=	performance index, [days]
$m_{\rm pay}$	=	payload mass, [kg]
$m_{\rm tot}$	=	total mass, [kg]
N	=	number of satellites
$\hat{\boldsymbol{n}}$	=	normal unit vector
$\hat{\boldsymbol{r}}$	=	radial unit vector
r	=	Sun-spacecraft distance, [au]
$r_\oplus$	=	reference distance equal to 1 au
t	=	time, [days]
$\{u, v\}$	=	spacecraft velocity components, [km/s]

*Corresponding author

Email addresses: lorenzo.niccolai@ing.unipi.it (Lorenzo Niccolai), andrea.caruso@ing.unipi.it (Andrea Caruso), a.quarta@ing.unipi.it (Alessandro A. Quarta), g.mengali@ing.unipi.it (Giovanni Mengali)

Published in Acta Astronautica, Vol. 177 December 2020, pp. 853–861. doi: https://doi.org/10.1016/j.actaastro.2019.12.003

$\boldsymbol{v}$	=	spacecraft velocity vector, [km/s]
α_n	=	pitch angle, [deg]
α_p	=	primer vector angle, [deg]
$\Delta\phi$	=	angular drift, [deg]
θ	=	angular coordinate, [deg]
$\{\lambda_r, \lambda_\theta, \lambda_u, \lambda_v\}$	=	adjoint variables
$\mu_\odot$	=	Sun's gravitational parameter, [km^3/s^2]
τ	=	switching parameter
ω	=	angular velocity, [rad/day]

Subscripts

0	=	initial
A	=	drift ahead
B	=	drift behind
f	=	final
i	=	i-th arc
max	=	maximum
tr	=	threshold value

Superscripts

$-$	=	design value
$\star$	=	optimal
$\cdot$	=	time derivative

1. Introduction

Since the dawn of space exploration, the study of the Sun and the main properties of the heliosphere have greatly attracted the interest of the scientific community [1, 2]. A first and obvious reason is that some catastrophic solar events, such as coronal mass ejections, could cause damages on orbiting spacecraft and even induce communication problems on Earth's surface. It is therefore important to implement ways of obtaining an early warning of such unpredictable events. A thorough understanding of solar behaviour could also increase our knowledge of other Sun-related phenomena, such as solar irradiance cycles and solar wind properties, which have a substantial impact on Earth's climate and on communication satellites. In this context, NASA's Parker Solar Probe [3] launched in August 2018, which will perform three (very) close passages by the star, is only the most recent example of a Sun-focused scientific mission. In fact, the first mission totally dedicated to the scientific investigation of the Sun's characteristics was Helios 1 [4], which provided relevant data on the solar wind and the corona. In 1980, NASA launched the Solar Maximum Mission [5], aimed at studying solar flares and high-energy components of the Sun's spectrum during its solar maximum, and a similar investigation was later conducted by the Japanese mission Yohkoh [6], launched in 1991. The lack of information about high-latitude solar zones was an important motivation for the successful Ulysses deep-space mission [7], which collected important data on the polar regions of the Sun [8].

More recently, three satellites have been placed in the vicinity of the L_1 collinear Lagrangian point of the Sun-Earth gravitational field [9]. In particular, NASA's Advanced Composition Explorer [10] is orbiting on a small-amplitude Lissajous orbit and is devoted to the study of solar wind and cosmic rays, whereas the Wind spacecraft mission [11] is mainly dedicated to analyzing the properties of the solar wind through *in-situ* measurements. Finally, the Solar and Heliospheric Observatory (SoHO) [12], a joint mission between ESA and NASA, is tracking a Halo orbit around L_1. SoHO is equipped with several scientific instruments that analyze the solar surface, its atmosphere, the corona, and solar wind as a part of the International Solar Terrestrial Physics Program, the aim of which is to improve the understanding of the physics of solar terrestrial relations. On a different but related point, propellantless propulsion systems have been also proposed for this kind of mission, in order to generate artificial orbits around stationary points closer to the Sun [13, 14, 15] than the natural Lagrange point.

A different approach for solar scientific investigations has been tested by the Solar Terrestrial Relations Observatory (STEREO) mission [16], launched in 2006 and operative until late 2014, although the periodic recovery operations ceased on October 2018. STEREO was made of two twin spacecraft, one (STEREO-A) drifting ahead of the Earth and one (STEREO-B) behind it, thus providing three-dimensional stereoscopic images of the Sun. The angular drift of the two satellites was obtained using a slightly different semimajor axis of their orbits, but a similar result could likewise be obtained by means of a heliocentric phasing maneuver, which could be performed by a spacecraft equipped with a propellantless propulsion system [17, 18].

This paper discusses in this respect the performance of an Electric Solar Wind Sail (or E-sail) [19], a recently-developed propellantless propulsion system, in a heliocentric mission scenario that requires a phasing maneuver. In its original configuration, an E-sail is constituted of a charged grid of spinning tethers, stretched out by the centrifugal force, and kept at a high positive potential; see Fig. 1(a). The E-sail generates a thrust by exploiting the electrostatic iteration between its charged grid of tethers and the incoming ions in the solar wind; see Fig. 1(b). The grid voltage is maintained by means of an electron gun, which expels the electrons attracted by the positively biased tethers. The required power consumption is on the order of some hundreds of watts [19], even for very large tether grids, and is therefore compatible with most spacecraft available power levels. However, due to the high complexity of the deployment mechanism of such large structures [20], other less complex configurations have been proposed, in which the propulsive acceleration is generated by a single or only a few tethers [21], although the working principle is essentially the same. Even though the original E-sail concept involves a positively-charged grid, the possibility of using a negatively-charged E-sail has been proposed by Janhunen [22]. The preliminary results obtained suggest its applicability even in a deep space mission, despite the existence of some technical complexities. In the case of negative polarity, the outwards thrust would be generated by the electrostatic interaction between the grid and the electrons in the solar wind. The recently proposed plasma-brake [23, 24, 25] is basically an application of this concept to a geocentric mission, in which a negatively-charged tether is used to deorbit a spacecraft from a low Earth orbit. Anyway, the analysis performed in this work would not be affected by a different polarity of the grid, since its main effect would be a modification of the E-sail performance parameter only.

The aim of this paper is to extend previous preliminary results [18] by means of the thrust model recently suggested by Huo et al. [27]. The analysis of a phasing maneuver can be addressed with two different strategies. The first one uses the Hill-Clohessy-Wiltshire equations [28], which model the relative motion between a spacecraft and its working heliocentric (circular) orbit. If the E-sail attitude is fixed with respect to an orbital reference frame, the integration of these equations provides a set of analytical expressions that give the spacecraft position as a function of time [29], in such a way that the flight time and the angular displacement can be calculated depending on the E-sail characteristics. However, such an approach has two important intrinsic limitations. First, its accuracy is limited by the assumption that the spacecraft remains close to the working orbit during the phasing maneuver. Moreover, it does not permit a variation of the E-sail attitude to be considered, and, for that reason, the phasing trajectories could be quite different from a truly optimal solution.

In this work, the heliocentric phasing maneuvers are therefore analyzed within an optimal framework, by minimizing the required flight time [30] and considering the nonlinear equations of motion of the E-sail-based spacecraft. In particular, the optimal control law of the E-sail attitude and the corresponding minimum maneuver time are obtained by means of an indirect approach. The system performance is analyzed in two different mission cases, that is, either a conventional phasing maneuver, or the deployment of a constellation of equally-spaced spacecraft on the same (circular) heliocentric orbit. Both scenarios are illustrated in the next section.

2. Problem description

A heliocentric phasing maneuver entails varying the angular position of a spacecraft along its reference (working) orbit, without affecting the other orbital parameters [31, 32]. Possible applications of phasing maneuvers include orbital rendezvous with a target object [33], active debris removal [34], and orbital repositioning on a given working orbit [35].

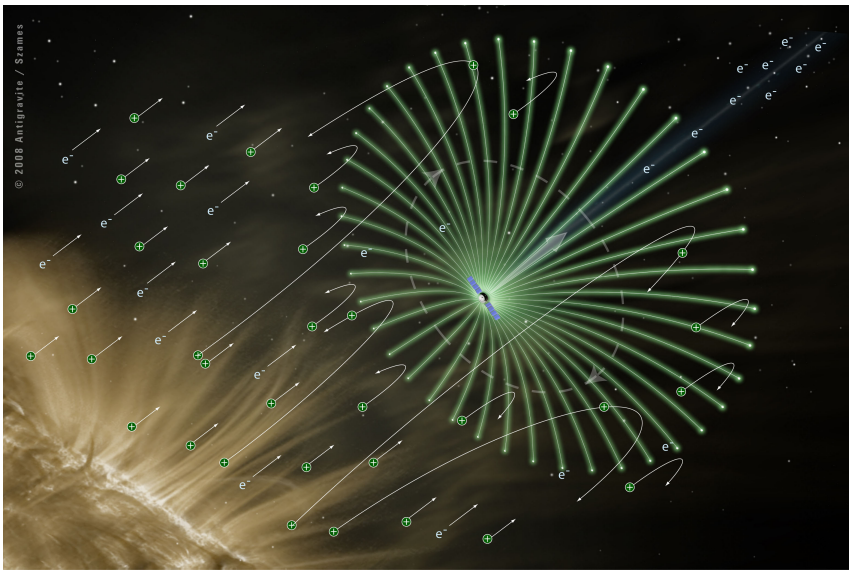

(a) Courtesy of Alexandre Szames, Antigravité (Paris).

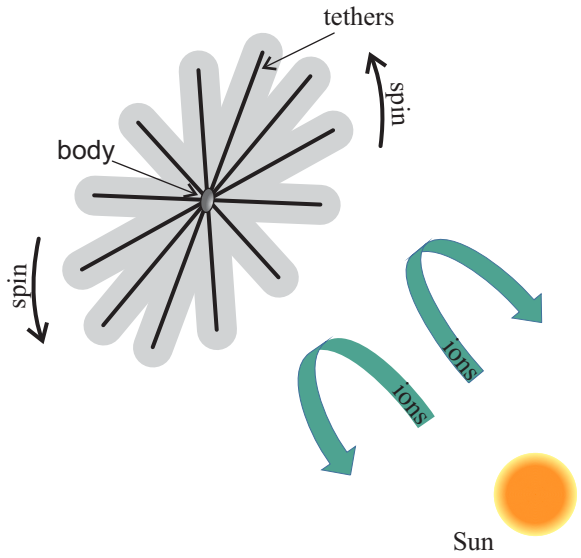

(b) Conceptual scheme.

Figure 1: Artistic rendering and conceptual sketch of an Electric Solar Wind Sail. Figure adapted from Ref. [26].

Phasing trajectories are usually classified into drift ahead or drift behind maneuvers. In the former case, the final spacecraft angular coordinate is greater than that of a virtual point that tracks the working orbit with a Keplerian motion. Likewise, in the latter case, this coordinate is smaller than that of the virtual point. These two cases are both shown in Fig. 2, which illustrates both a drift ahead and a drift behind maneuver with respect to the Earth, assuming that the spacecraft leaves the Earth's sphere of influence with zero excess velocity relative to it.

Typically, a phasing trajectory on a circular working orbit may be obtained in a very simple way with a bi-impulsive maneuver by means of a chemical thruster, in which the two impulses give the same velocity variation and are both tangentially directed. This approach, however, usually requires a significant value of velocity variation and, therefore, a large amount of propellant consumption. Accordingly, the possibility of exploiting a low-thrust propellantless propulsion system in this mission scenario is an interesting option.

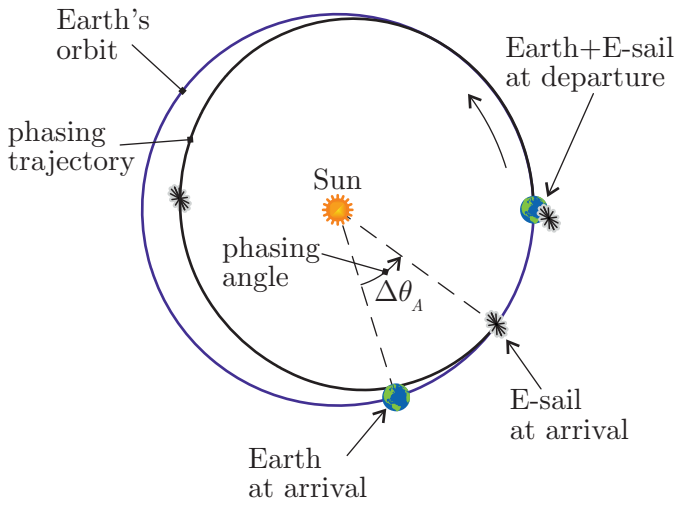

(a) Drift ahead.

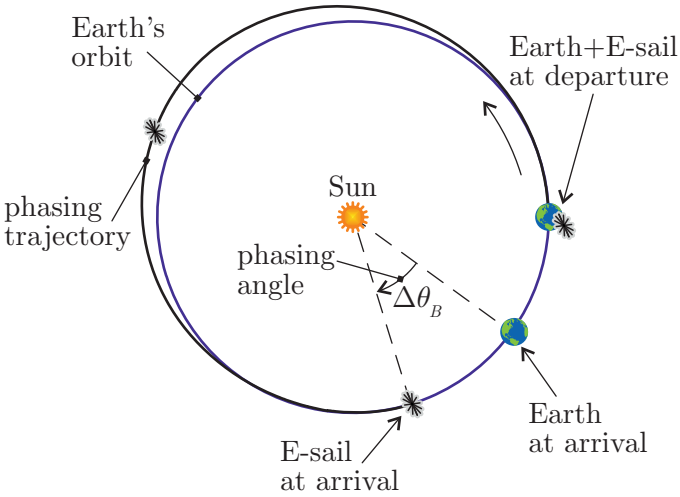

(b) Drift behind.

Figure 2: Conceptual sketch of a phasing maneuver on the Earth's heliocentric orbit.

In particular, the problem of investigating a solar-sail-enabled phasing maneuver has been investigated at length in the literature [36, 17, 37], with possible applications involving a Smart Dust [29, 35], that is, a miniaturized femtosatellite with a high area-to-mass ratio [38]. Some results also exist for a spacecraft propelled by an E-sail [18], even though they were obtained with a quite simplified thrust model that is based on the assumption that the propulsive acceleration magnitude is independent of the spacecraft attitude.

A special application of a set of (consecutive) phasing maneuvers consists in a constellation deployment by means of a sort of "deployer" spacecraft. Such a mission involves an E-sail-based shuttle, the payload of which is constituted by $N \geq 2$ small satellites, each one being equipped with suitable scientific instrumentation. The constellation deployment is achieved by means of succeeding heliocentric phasing maneuvers. In particular, at the end of each phasing trajectory arc, one of the satellites stowed in the deployer is ejected (with zero velocity relative to it). Once the whole payload has been ejected from the shuttle, the deployment phase ends, and the satellites are all placed on the same heliocentric (working) orbit with a prescribed

angular separation, thus enabling a scientific observation of the Sun from different locations. A sketch of a constellation deployment scenario is shown in Fig. 3. Such an idea may be considered as a potential extension of the STEREO mission concept [16].

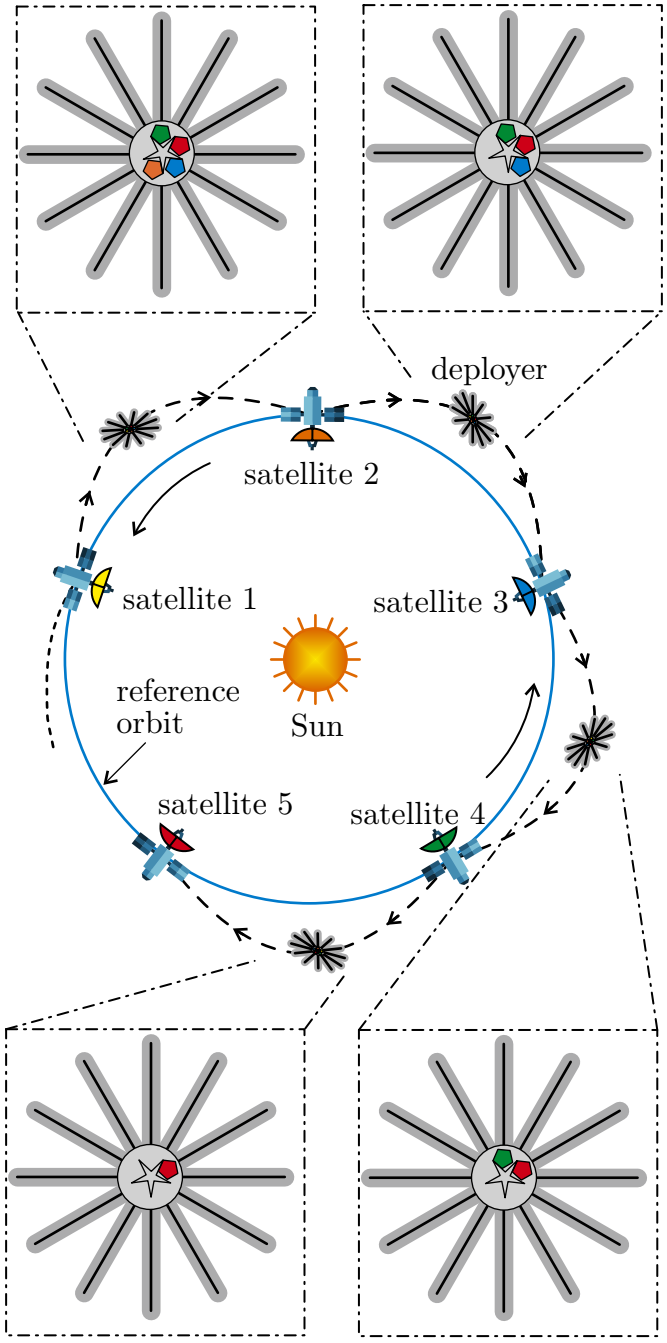

Figure 3: Conceptual sketch of a constellation deployment scenario by means of an E-sail-based deployer.

3. Mathematical model

According to the recent results by Huo et al. [27], the propulsive acceleration vector $\boldsymbol{a}$ generated by a flat, disc-shaped E-sail may be written in a compact analytical form as

$$\boldsymbol{a} = \tau \, \frac{a_c}{2} \left(\frac{r_\oplus}{r} \right) \left[\hat{\boldsymbol{r}} + (\hat{\boldsymbol{r}} \cdot \hat{\boldsymbol{n}}) \, \hat{\boldsymbol{n}} \right] \tag{1}$$

where $\tau \in \{0, 1\}$ is a dimensionless parameter that accounts for the possibility of switching either on ($\tau = 1$) or off ($\tau = 0$) the electron gun that maintains the E-sail (positive) grid voltage, $r_\oplus \triangleq 1\,\text{au}$ is a reference distance, $\hat{\boldsymbol{r}}$ is the Sun-spacecraft unit vector (with $r = \|\boldsymbol{r}\|$), and $\hat{\boldsymbol{n}}$ is the unit vector normal to the E-sail nominal plane and directed outwards with respect to the Sun; see Fig. 4. In Eq. (1), a_c is the characteristic

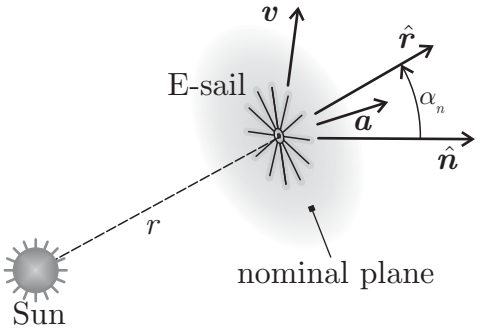

Figure 4: Conceptual sketch of the vectors involved in E-sail thrust generation. Adapted from Ref. [39]

acceleration, which depends on the grid voltage and the sail design parameters, and is usually chosen as the reference performance parameter for an E-sail-based spacecraft. The assumption of a constant value of a_c implies that the variations of the solar wind properties are neglected to a first order. The interested reader may find more details on this topic in Refs. [40, 39, 41], which discuss the effects of the solar wind dynamic pressure variation on the characteristic acceleration value. Note that Eq. (1) also assumes that the E-sail tethers belong to same plane (that is, the E-sail has an ideal flat shape), in accordance with the recent results stating that the thrust magnitude reduction caused by tether inflection is negligible [42, 43]. In particular, the thrust model of Eq. (1) gives a propulsive acceleration vector $\boldsymbol{a}$, whose maximum inclination with respect to the radial direction is about 19.5 deg. Such a result has been obtained first by numerical simulations [44] and then derived analytically in Ref. [27], starting from the preliminary results of Ref. [45]. A thorough description of the E-sail thrust direction constraint (and, in general, of the adopted thrust model) may be found in Ref. [27].

Consider an E-sail-based spacecraft which covers a heliocentric, circular working orbit of radius r_0. Assume that the propulsive acceleration vector $\boldsymbol{a}$ belongs to the working orbit plane, and introduce a polar heliocentric reference frame $\mathcal{T}(O; r, \theta)$ of unit vector $\hat{\boldsymbol{i}}_r \equiv \hat{\boldsymbol{r}}$ and $\hat{\boldsymbol{i}}_\theta$, whose origin coincides with the Sun's center-of-mass O. In particular, θ is the azimuthal angle measured counterclockwise from a given (fixed) direction that coincides with the initial Sun-spacecraft line; see Fig. 5.

Taking into account that the spacecraft motion is two-dimensional, from Eq. (1) the radial (a_r) and circumferential (a_θ) components of the propulsive acceleration may be written as

$$a_r \triangleq \boldsymbol{a} \cdot \hat{\boldsymbol{i}}_r = \tau \, \frac{a_c}{4} \left(\frac{r_\oplus}{r} \right) \left[3 + \cos(2\,\alpha_n) \right] \tag{2}$$

$$a_\theta \triangleq \boldsymbol{a} \cdot \hat{\boldsymbol{i}}_\theta = \tau \, \frac{a_c}{4} \left(\frac{r_\oplus}{r} \right) \sin(2\,\alpha_n) \tag{3}$$

where $\alpha_n \in [-90, 90]\,\text{deg}$ is the sail pitch angle defined as the angle between the direction of $\hat{\boldsymbol{r}}$ and that of $\hat{\boldsymbol{n}}$, viz.

$$\alpha_n \triangleq \text{sign}(\boldsymbol{v} \cdot \hat{\boldsymbol{n}}) \, \arccos(\hat{\boldsymbol{r}} \cdot \hat{\boldsymbol{n}}) \tag{4}$$

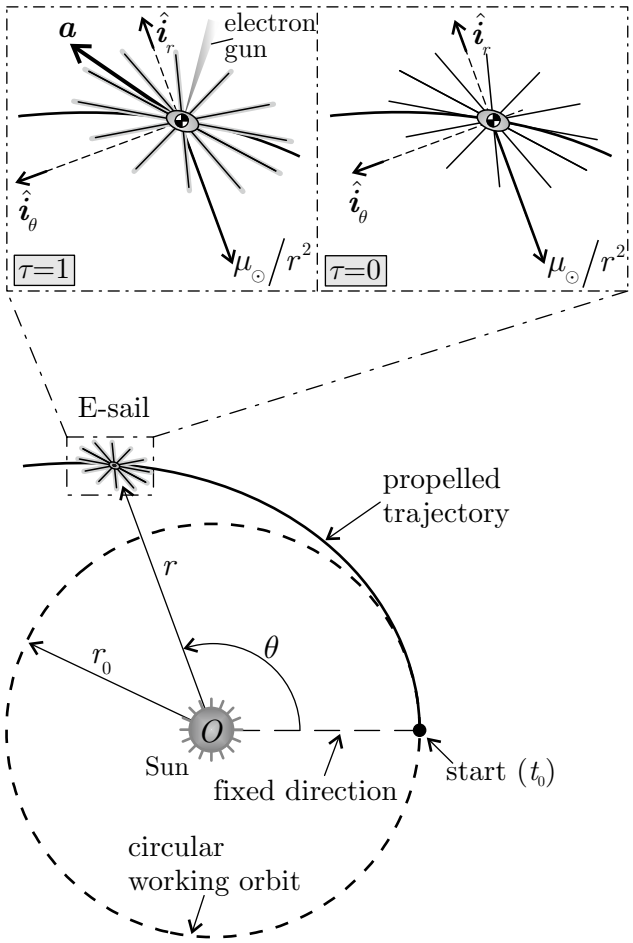

Figure 5: Reference frame and spacecraft state variable.

where $\boldsymbol{v}$ is the spacecraft velocity vector, and sign $(\square)$ is the signum function. In the rest of the analysis, it is assumed that the sail pitch angle α_n can be varied by adjusting the voltage level of tethers with a suitable control law, as proposed in Refs. [46, 47].

Bearing in mind Eqs. (2) and (3), the spacecraft dynamics in the polar reference frame $\mathcal{T}$ can be written as

$$\dot{r} = u \tag{5}$$

$$\dot{\theta} = v/r \tag{6}$$

$$\dot{u} = -\frac{\mu_\odot}{r^2} + \frac{v^2}{r} + \tau \, \frac{a_c}{4} \left(\frac{r_\oplus}{r}\right) \left[3 + \cos\left(2\,\alpha_n\right)\right] \tag{7}$$

$$\dot{v} = -\frac{u\,v}{r} + \tau \, \frac{a_c}{4} \left(\frac{r_\oplus}{r}\right) \sin\left(2\,\alpha_n\right) \tag{8}$$

where the dot symbol denotes a time derivative, $\mu_\odot$ is the Sun's gravitational parameter, and u and v are the radial and circumferential components of the spacecraft velocity vector $\boldsymbol{v}$. According to Eqs. (5)–(8), the spacecraft (two-dimensional) motion is described by the four state variables $\{r,\, \theta,\, u,\, v\}$ and the two control variables $\{\tau,\, \alpha_n\}$.

3.1. Trajectory optimization

Let the state variables at the initial time $t_0 \triangleq 0$ be

$$r(t_0) = r_0, \quad \theta(t_0) = 0, \quad u(t_0) = 0, \quad v(t_0) = \sqrt{\mu_\odot / r_0} \tag{9}$$

where the angular coordinate $\theta(t_0)$ has been set to zero, without loss of generality, because the working orbit is circular. The optimization of a phasing maneuver consists in looking for the control law that minimizes the time $\Delta t \triangleq t_f - t_0 \equiv t_f$ required for the spacecraft to track the same initial (circular) orbit, but with an angular drift $\Delta\phi \in [0,\, 360)\,\mathrm{deg}$. The latter is measured at t_f counterclockwise from the line connecting the Sun and a virtual point that has continued tracking the nominal (Keplerian) orbit from t_0 to t_f. In other terms, the boundary conditions at time t_f are given by

$$r(t_f) = r_0, \quad \theta(t_f) = \omega_0\, t_f + \Delta\phi, \quad u(t_f) = 0, \quad v(t_f) = \sqrt{\mu_\odot / r_0} \tag{10}$$

where $\omega_0 \triangleq \sqrt{\mu_\odot / r_0^3}$ is the angular velocity on the working orbit. In particular, denoting with either $\Delta\theta_A$ or $\Delta\theta_B$ the absolute value of the angular variation in a drift ahead or a drift behind maneuver, respectively, $\Delta\phi$ is defined as

$$\Delta\phi \triangleq \begin{cases} \Delta\theta_A & \text{drift ahead case} \\ 360\,\mathrm{deg} - \Delta\theta_B & \text{drift behind case} \end{cases} \tag{11}$$

in accordance with Fig. 2.

The minimum-time trajectory corresponding to the phasing maneuver with boundary conditions (9) and (10), is obtained by maximizing the performance index

$$J \triangleq -t_f \tag{12}$$

The dynamical system defined by Eqs. (5)–(8) admits an Hamiltonian function $\mathcal{H}$, defined as

$$\mathcal{H} \triangleq \lambda_r\, u + \lambda_\theta\, \frac{v}{r} + \lambda_u \left(-\frac{\mu_\odot}{r^2} + \frac{v^2}{r} + a_r \right) + \lambda_v \left(-\frac{u\, v}{r} + a_\theta \right) \tag{13}$$

where a_r and a_θ are given by Eqs. (2) and (3), while λ_r, λ_θ, λ_u, and λ_v denote the adjoint variables associated with the state variables r, θ, u, and v. Their time derivatives are given by the Euler-Lagrange equations as

$$\dot\lambda_r \triangleq -\frac{\partial \mathcal{H}}{\partial r} = \lambda_\theta\, \frac{v}{r^2} + \lambda_u \left(\frac{v^2}{r^2} - \frac{2\,\mu_\odot}{r^3} + \frac{a_r}{r} \right) + \lambda_v \left(-\frac{u\, v}{r^2} + \frac{a_\theta}{r} \right) \tag{14}$$

$$\dot\lambda_\theta \triangleq -\frac{\partial \mathcal{H}}{\partial \theta} = 0 \tag{15}$$

$$\dot\lambda_u \triangleq -\frac{\partial \mathcal{H}}{\partial u} = -\lambda_r + \lambda_v\, \frac{v}{r} \tag{16}$$

$$\dot\lambda_v \triangleq -\frac{\partial \mathcal{H}}{\partial v} = -\lambda_\theta\, \frac{1}{r} - 2\,\lambda_u\, \frac{v}{r} + \lambda_v\, \frac{u}{r} \tag{17}$$

In particular, Eq. (15) states that λ_θ is a constant of motion.

The optimal phasing trajectory is the solution of a two-point boundary value problem (TPBVP), constituted by the equations of motion (5)–(8) and the Euler-Lagrange equations (14)–(17), with four boundary conditions at $t = t_0$ given by Eqs. (9), and four at $t = t_f$ given by Eqs. (10). The final (minimum) time t_f is obtained by enforcing the transversality condition [48], which is obtained from Eq. (12) and the second of Eqs. (10) as

$$\mathcal{H}(t_f) = 1 + \lambda_\theta \sqrt{\frac{\mu_\odot}{r_0^3}} \tag{18}$$

Using the Pontryagin's maximum principle, the optimal control law $\tau = \tau^\star(t)$ and $\alpha_n = \alpha_n^\star(t)$ are found by maximizing, at each time instant t, the Hamiltonian function given by Eq. (13). Bearing in mind the

geometric approach discussed in Ref. [27], the optimal control law can be written as

$$\tau^\star = \frac{1 + \text{sign}\,(1 + 3\,\cos\alpha_p)}{2} \tag{19}$$

$$\alpha_n^\star = \frac{\alpha_p}{2} \tag{20}$$

where the angle $\alpha_p \in [-180, 180]\,\text{deg}$, defined as

$$\alpha_p \triangleq \text{sign}\,(\lambda_v)\,\arccos\left(\frac{\lambda_u}{\sqrt{{\lambda_u}^2 + {\lambda_v}^2}}\right) \tag{21}$$

denotes the angle between the Lawden's primer vector [49] $\boldsymbol{\lambda_v} \triangleq [\lambda_u,\, \lambda_v]^{\text{T}}$ and the radial direction.

4. Numerical simulations

The time-optimal phasing maneuvers performed by an E-sail have been investigated with numerical simulations, in which the differential equations have been integrated in double precision by means of a variable order Adams-Bashforth-Moulton solver scheme [50, 51] with absolute and relative errors of 10^{-12}.

4.1. Phasing maneuvers

As a first exemplary case, consider a spacecraft propelled by a low-performance E-sail with characteristic acceleration $a_c = 0.1\,\text{mm/s}^2$. The reference orbit coincides with the Earth's (circular) heliocentric orbit ($r_0 = r_\oplus$). This case corresponds to a situation in which the spacecraft leaves the planet's sphere of influence with zero excess velocity. Figure 6 shows the minimum flight time t_f as a function of the angular drift $\Delta\phi$ given by Eq. (11), in both cases of either drift ahead or drift behind maneuvers.

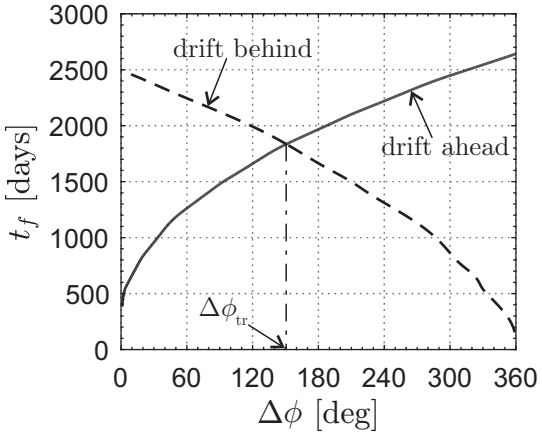

Figure 6: Minimum flight time t_f as a function of the angular drift $\Delta\phi$ when $a_c = 0.1\,\text{mm/s}^2$.

Each value of $\Delta\phi$ can be obtained, in principle, both with a drift ahead and a drift behind maneuver. When only the magnitude of the angular drift is relevant for the mission requirements, considering either a drift ahead maneuver with angular change $\Delta\overline{\theta}_A$ or a drift behind maneuver with $\Delta\overline{\theta}_B = \Delta\overline{\theta}_A$, the latter choice is better (that is, smaller) in terms of flight time. However, when a given angular displacement $\Delta\phi$ must be obtained (see Eq. (11)), a drift ahead maneuver could be more convenient, in particular for small values of $\Delta\phi$. There exists, however, a threshold value, beyond which a drift behind maneuver requires a smaller flight time. This is clearly illustrated in Fig. 6, from which the value of $\Delta\phi_{\text{tr}}$ is about 150.7 deg when $a_c = 0.1\,\text{mm/s}^2$. The global minimum of the flight time, for both cases of drift ahead and drift behind maneuvers, is reported in Figure 7 as a function of $\Delta\phi$. The maximum flight time is obtained when $\Delta\phi = \Delta\phi_{\text{tr}}$ and is equal to $t_{f_{\max}} = 1836\,\text{days} \simeq 5\,\text{years}$.

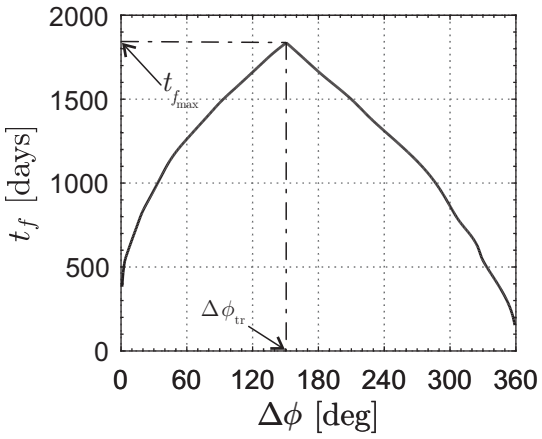

Figure 7: Global minimum of the flight time t_f as a function of the angular drift $\Delta\phi$ when $a_c = 0.1\,\text{mm/s}^2$.

4.2. Constellation deployment scenario

The constellation deployment scenario has been described in Section 2. Assume a deployer payload mass $m_{\text{pay}} = 100\,\text{kg}$, which coincides with the total mass of the N spacecraft stowed within it, and consider an initial characteristic acceleration $a_c = \{0.1,\, 1\}\,\text{mm/s}^2$. According to the E-sail mass budget model of Ref. [52], these performance parameters could be achieved by a spacecraft with a total in-flight mass of $m_{\text{tot}} = \{280,\, 391\}\,\text{kg}$. In particular, the results of Ref. [52] suggest that an E-sail with $a_c = 0.1\,\text{mm/s}^2$ and $m_{\text{pay}} = 100\,\text{kg}$ should be equipped with 12 tethers with a length of about 4 km each, so its mass would be 31.7 kg. The estimated power consumption is 38.5 W only. For comparative purposes, a high-performance deployer with $a_c = 1\,\text{mm/s}^2$ and $m_{\text{pay}} = 100\,\text{kg}$ should be propelled by an E-sail with 44 tethers, with a length of about 15 km each. The total E-sail mass would be 143 kg, with a total power consumption on the order of 400 W.

The constellation deployment can be seen as a succession of consecutive phasing maneuvers with the same angular drift and with identical boundary conditions as those of Eqs. (9) and (10). This is a consequence of the assumption that the reference orbit is circular, so that the initial value of the angular coordinate may be freely chosen. Assuming that the first satellite is released in proximity of Earth (just outside its sphere of influence), the trajectory tracked by the deployer is composed of $N-1$ arcs. The angular drift in each arc depends on the number N of satellites stowed in the deployer. Indeed, if a constellation with equally-spaced elements must be obtained, the angular drift in the generic i-th trajectory arc is

$$\Delta\theta_{B_i} = \frac{360}{N}\,\text{deg} \qquad \text{for} \qquad i = 1, 2, \ldots, N-1 \tag{22}$$

where a drift behind maneuver is assumed, based on the previously discussed results. The value of $\Delta\phi_i$ is obtained by substituting Eq. (22) into Eq. (11). Note that the spacecraft characteristic acceleration has a discontinuity at each deployment time t_{fi}, due to the instantaneous reduction of the total deployer mass. In particular, the characteristic acceleration a_{c_i} during the i-th trajectory arc is given by

$$a_{c_i} = a_c\,\frac{m_{\text{tot}}}{m_{\text{tot}} - m_{\text{pay}}(i/N)} \qquad \text{for} \qquad i = 1, 2, \ldots, N-1 \tag{23}$$

where $a_{c_0} \equiv a_c$ is the initial value of characteristic acceleration. Finally, the total maneuver time is simply the sum of all the time intervals required to perform each phasing maneuver, viz.

$$t_f = \sum_{i=1}^{N-1} t_{f_i} \tag{24}$$

Figure 8 shows the values of t_{f_i} as a function of the (initial) characteristic acceleration a_c and the total number of satellites N. Once the E-sail characteristic acceleration in the i-th arc is found with

Eq. (23), the flight time t_{f_i} is obtained graphically from Fig. 8 as a function of N. Finally, the total time for the constellation deployment is given by Eq. (24). Table 1 summarizes the results for an E-sail-based constellation deployment for different numbers of satellites N, assuming an initial characteristic acceleration $a_c = 0.1\,\mathrm{mm/s^2}$.

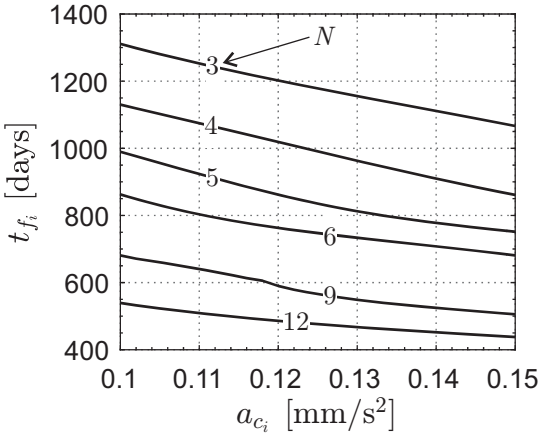

(a) $a_c = 0.1\,\mathrm{mm/s^2}$

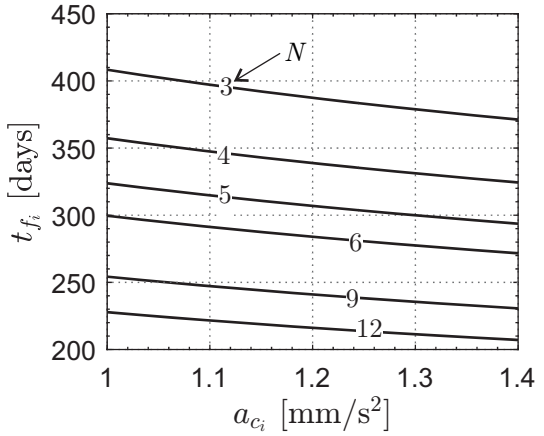

(b) $a_c = 1\,\mathrm{mm/s^2}$

Figure 8: Time required to accomplish an arc of the constellation deployment mission $t_{f_i} = t_{f_i}(a_{c_i}, N)$ when $a_c = \{0.1,\, 1\}\,\mathrm{mm/s^2}$.

$\Delta\theta_{B_i}$ [deg]	N	t_f [days]
120	3	2385
90	4	3012
72	5	3428
60	6	3799
40	9	4685
30	12	5315

Table 1: Constellation deployment performance as a function of N when $a_c = 0.1\,\mathrm{mm/s^2}$.

The deployment of a considerable number of satellites requires a very high value of t_f. Indeed, even assuming that the deployer contains just three satellites (i.e. $N = 3$), the total deployment time amounts

to more than 6 years. However, the mission time could be substantially shortened by increasing the E-sail performance. This is clearly illustrated in Tab. 2, which reports the same cases as those of Tab. 1, but now assuming $a_c = 1\,\mathrm{mm/s^2}$.

$\Delta\theta_{B_i}$ [deg]	N	t_f [days]
120	3	785
90	4	1030
72	5	1241
60	6	1438
40	9	1953
30	12	2407

Table 2: Constellation deployment performance as a function of N when $a_c = 1\,\mathrm{mm/s^2}$.

For example, if the deployer inserts $N = 3$ equally-spaced spacecraft on the reference orbit (i.e. $\Delta\theta_{B_i} = 120\,\mathrm{deg}$), the total mission time reduces to 785 days $\simeq 2.15$ years. The corresponding trajectory is sketched in Fig. 9, which shows that the optimal transfer trajectory includes also coasting (Keplerian) arcs, in which $\tau = 0$.

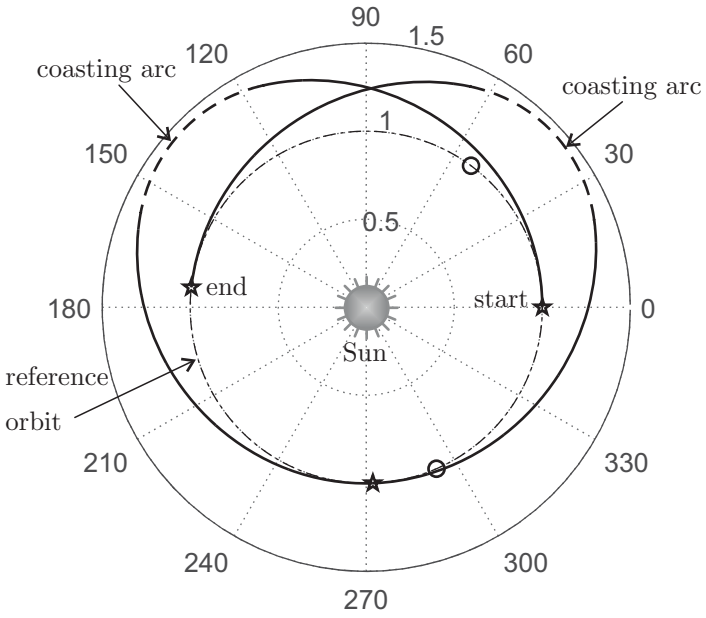

Figure 9: Constellation deployment trajectory with $a_c = 1\,\mathrm{mm/s^2}$ and $N = 3$ (propelled arc: solid line; coasting arc: dash line; satellite releases: stars; deployed satellite position at t_f: circles).

5. Conclusions

This work has presented a preliminary analysis of an optimal phasing maneuver along a circular heliocentric orbit performed by means of an Electric Solar Wind Sail-based spacecraft. Taking into account that such an advanced propulsion system is propellantless, time-optimal phasing trajectories have been investigated in both cases of drift ahead and drift behind maneuvers. In particular, for a given (fixed) angular displacement, a drift behind maneuver is the most convenient option in terms of required time.

A special application of phasing maneuvers has been proposed, which consists in a constellation deployment scenario by means of a sort of deployer spacecraft propelled by an Electric Solar Wind Sail. In particular, the deployer releases the generic satellite along the (same) working orbit with zero relative velocity. In this context, the simulation results suggest that a constellation of equally-spaced satellites could be inserted along a heliocentric orbit of radius equal to one astronomical unit, even though the total required time assumes a reasonable value only using a medium- or high-performance sail.

Acknowledgments

This work is supported by the University of Pisa, Progetti di Ricerca di Ateneo (Grant no. PRA 2018 44).

References

[1] M. P. Thekaekara, The solar constant and spectral distribution of solar radiant flux, Solar Energy 9 (1) (1965) 7–20, doi: 10.1016/0038-092X(65)90155-6.
[2] H. E. Hinteregger, Absolute intensity measurements in the extreme ultraviolet spectrum of solar radiation, Space Science Reviews 4 (4) (1965) 461–497, doi: 10.1007/BF00177091.
[3] A. Szabo, Flying into the Sun, Nature Astronomy 2 (10) (2018) 829, doi: 10.1038/s41550-018-0580-3.
[4] M. Howard, Project helios, Spaceflight 17 (5) (1975) 184–188 .
[5] E. Chipman, Overview of NASA solar physics programs, Proceedings of SPIE - The International Society for Optical Engineering 184 (1979) 256–263, doi: 10.1117/12.957459.
[6] L. Acton, S. Tsuneta, Y. Ogawara, et al., The yohkoh mission for high-energy solar physics, Science 258 (5082) (1992) 618–625, doi: 10.1126/science.258.5082.618.
[7] K.-P. Wenzel, R. G. Mardsen, D. E. Page, E. J. Smith, Ulysses: The first high-latitude heliospheric mission, Advances in Space Research 9 (4) (1989) 25–29, doi: 10.1016/0273-1177(89)90089-6.
[8] J. L. Phillips, S. J. Bame, A. Barnes, Ulysses solar wind plasma observation from pole to pole, Geophysical Research Letters 22 (23) (1995) 3301–3304, doi: 10.1029/95GL03094.
[9] C. E. Roberts, Long term mission at the Sun-Earth libration point L1: ACE, SOHO, and WIND, Advances in the Astronautical Sciences 142 (2012) 1263–1282 .
[10] E. C. Stone, A. M. Frandsen, R. A. Mewaldt, E. R. Christian, D. Margolies, J. F. Ormes, F. Snow, The Advanced Composition Explorer, Space Science Reviews 86 (1–4) (1998) 1–22 .
[11] H. Franz, P. J. Sharer, K. Ogilvie, M. Desch, WIND nominal mission performance and extended mission design, in: AIAA/AAS Astrodynamics Specialist Conference and Exhibit, Boston, MA, USA, 1998.
[12] D. W. Dunham, S. J. Jen, C. E. Roberts, A. W. Seacord, P. J. Sharer, D. C. Folta, D. P. Muhonen, Transfer trajectory design for the SOHO libration-point mission, in: 43rd International Astronautical Congress, Washington, DC, USA, 1992.
[13] G. Vulpetti, C. Circi, T. Pino, Coronal Mass Ejection early-warning mission by solar-photon sailcraft, Acta Astronautica 140 (2017) 113–125, doi: 10.1016/j.actaastro.2017.07.042.
[14] L. Niccolai, A. A. Quarta, G. Mengali, Electric sail elliptic displaced orbit with advanced thrust model, Acta Astronautica 138 (2017) 503–511, doi: 10.1016/j.actaastro.2016.10.036.
[15] L. Niccolai, A. A. Quarta, G. Mengali, Electric sail-based displaced orbits with a refined thrust model, Proceedings of the Institution of Mechanical Engineers, Part G: Journal of Aerospace Engineering 232 (3) (2018) 423–432, doi: 10.1177/0954410016679195.
[16] M. L. Kaiser, The STEREO mission: An overview, Advances in Space Research 36 (8) (2005) 1483–1488, doi: 10.1016/j.asr.2004.12.066.
[17] G. Mengali, A. A. Quarta, In-orbit repositioning of multiple solar sail spacecraft, Aerospace Science and Technology 12 (7) (2008) 506–514, doi: 10.1016/j.ast.2007.12.003.
[18] G. Mengali, A. A. Quarta, G. Aliasi, Heliocentric phasing performance of electric sail spacecraft, Acta Astronautica 127 (2016) 474–481, doi: 10.1016/j.actaastro.2016.06.033.
[19] P. Janhunen, Electric sail for spacecraft propulsion, Journal of Propulsion and Power 20 (4) (2004) 763–764, doi: 10.2514/1.8580.
[20] J. Fulton, H. Schaub, Fixed-axis electric sail deployment dynamics analysis using hub-mounted momentum control, Acta Astronautica 144 (2018) 160–170, doi: 10.1016/j.actaastro.2017.11.048.
[21] C. Montalvo, B. Wiegmann, Electric sail space flight dynamics and controls, Acta Astronautica 148 (2018) 268–275, doi: 10.1016/j.actaastro.2018.05.009.
[22] P. Janhunen, On the feasibility of a negative polarity electric sail, Annales Geophysicae 27 (4) (2009) 1439–1447, doi: 10.5194/angeo-27-1439-2009.
[23] P. Janhunen, Simulation study of the plasma-brake effect, Annales Geophysicae 32 (10) (2014) 1207–1216, doi: 10.5194/angeo-32-1207-2014.
[24] I. Iakubivsky, H. Ehrpais, J. Dalbins, et al., Estcube-2 mission analysis: Plasma brake experiment for deorbiting, in: 67th International Astronautical Congress, Guadalajara, Mexico, 2016.
[25] L. Orsini, L. Niccolai, G. Mengali, A. A. Quarta, Plasma brake model for preliminary mission analysis, Acta Astronautica 144 (2018) 297–304, doi: 10.1016/j.actaastro.2017.12.048.
[26] L. Niccolai, A. A. Quarta, G. Mengali, F. Petrucciani, Possible trajectories for electric solar wind sail validation, Aerotecnica Missili & Spazio 98 (2) (2019) 139–145, doi: 10.1007/s42496-019-00012-7.

[27] M. Huo, G. Mengali, A. A. Quarta, Electric sail thrust model from a geometrical perspective, Journal of Guidance, Control, and Dynamics 41 (2018) 734–740, doi: 10.2514/1.G003169.
[28] W. Clohessy, R. Wiltshire, Terminal guidance system for satellite rendezvous, Journal of the Aerospace Sciences 270 (1960) 653–674 .
[29] G. Mengali, A. A. Quarta, E. Denti, Relative motion of Sun-pointing Smart Dust in circular heliocentric orbits, Journal of Guidance, Control, and Dynamics 41 (4) (2018) 1009–1014, doi: 10.2514/1.G003088.
[30] A. A. Quarta, G. Mengali, Minimum-time trajectories of electric sail with advanced thrust model, Aerospace Science and Technology 55 (2016) 419–430, doi: 10.1016/j.ast.2016.06.020.
[31] V. A. Chobotov, Orbital Mechanics, 3rd Edition, American Institute of Aeronautics and Astronautics, 2002, Ch. 7, pp. 152–155.
[32] H. D. Curtis, Orbital Mechanics for Engineering Students, Butterworth-Heinemann, 2014, Ch. 6, pp. 312–317.
[33] R. F. Murtazin, S. G. Budylov, Short rendezvous mission for advanced Russian human spacecraft, Acta Astronautica 67 (7–8) (2010) 900–909, doi: 10.1016/j.actaastro.2010.05.012.
[34] J. Yu, X. Q. Chen, L. H. Chen, D. Hao, Optimal scheduling of GEO debris removing based on hybrid optimal control theory, Acta Astronautica 93 (2014) 400–409, doi: 10.1016/j.actaastro.2013.07.015.
[35] A. A. Quarta, G. Mengali, E. Denti, Optimal in-orbit repositioning of Sun-pointing Smart Dust, Acta Astronautica 154 (2019) 278–285, doi: 10.1016/j.actaastro.2018.03.036.
[36] C. R. McInnes, Azimuthal repositioning of payloads in heliocentric orbit using solar sails, Journal of Guidance, Control, and Dynamics 26 (4) (2003) 662–664, doi: 10.2514/2.5098.
[37] A. A. Quarta, G. Mengali, Optimal solar sail phasing trajectories for circular orbit, Journal of Guidance, Control, and Dynamics 36 (6) (2013) 1821–1824, doi: 10.2514/1.59372.
[38] L. Niccolai, M. Bassetto, A. A. Quarta, G. Mengali, A review of smart dust architecture, dynamics, and mission applications, Progress in Aerospace Sciences 106 (2019) 1–14, doi: 10.1016/j.paerosci.2019.01.003.
[39] L. Niccolai, A. Anderlini, G. Mengali, A. A. Quarta, Impact of solar wind fluctuations on electric sail mission design, Aerospace Science and Technology 82–83 (2018) 38–45, doi: 10.1016/j.ast.2018.08.032.
[40] P. K. Toivanen, P. Janhunen, Electric sailing under observed solar wind conditions, Astrophysics and Space Sciences Transactions 5 (1) (2009) 61–69, doi: 10.5194/astra-5-61-2009.
[41] L. Niccolai, A. Anderlini, G. Mengali, A. A. Quarta, Electric sail displaced orbit control with solar wind uncertainties, In press. Acta Astronautica .
[42] M. Bassetto, G. Mengali, A. A. Quarta, Thrust and torque vector characteristics of axially-symmetric e-sail, Acta Astronautica 146 (2018) 134–143, doi: 10.1016/j.actaastro.2018.02.035.
[43] M. Bassetto, G. Mengali, A. A. Quarta, Stability and control of spinning elecric solar wind sail in heliostationary orbit, Journal of Guidance, Control and Dynamics 42 (2) (2019) 425–431, doi: 10.2514/1.G003788.
[44] K. Yamaguchi, H. Yamakawa, Study on orbital maneuvers for electric sail with on-off thrust control, Aerospace Technology Japan 12 (2013) 79–88, doi: 10.2322/astj.12.79.
[45] P. Janhunen, The electric solar wind sail status report, in: European Planetary Science Congress, Vol. 5, 2010.
[46] P. K. Toivanen, P. Janhunen, J. Envall, Electric sail control mode for amplified transverse thrust, Acta Astronautica 106 (2015) 111–119, doi: 10.1016/j.actaastro.2014.10.031.
[47] M. Bassetto, G. Mengali, A. A. Quarta, Attitude dynamics of an electric sail model with a realistic shape, Acta Astronautica 159 (2019) 250–257, doi: 10.1016/j.actaastro.2019.03.064.
[48] A. E. Bryson, Y. C. Ho, Applied Optimal Control, Hemisphere Publishing Corporation, 1975, Ch. 2, pp. 71–89.
[49] D. F. Lawden, Optimal Trajectories for Space Navigation, Butterworths & Co., London, 1963, pp. 54–60.
[50] L. F. Shampine, M. K. Gordon, Computer Solution of Ordinary Differential Equations: The Initial Value Problem, W. H. Freeman & Co Ltd, San Francisco, 1975, Ch. 10, ISBN: 0-716-70461-7.
[51] L. F. Shampine, M. W. Reichelt, The MATLAB ODE suite, SIAM Journal on Scientific Computing 18 (1) (1997) 1–22, doi: 10.1137/S1064827594276424.
[52] P. Janhunen, A. A. Quarta, G. Mengali, Electric solar wind sail mass budget model, Geoscientific Instrumentation, Methods and Data Systems 2 (1) (2013) 85–95, doi: 10.5194/gi-2-85-2013.